

Sarah M. Stough<sup>1\*</sup>, Lawrence D. Carey<sup>1</sup>, Christopher J. Schultz<sup>2</sup>, and Daniel J. Cecil<sup>2</sup>

1. Department of Atmospheric Science, University of Alabama in Huntsville, Huntsville, Alabama
2. Earth Science Office, NASA Marshall Space Flight Center, Huntsville, Alabama

## 1. INTRODUCTION

The updraft has been recognized for some time as the physical basis of the observed relationship between rapid increases in lightning flash rates, or lightning jumps, and severe weather. Numerous studies have observed and further analyzed the microphysical and kinematic basis of the relationship between severe weather, lightning flash rates, and lightning jumps (e.g., MacGorman et al. 1989; Carey and Rutledge 1996; Williams et al. 1999; Lang and Rutledge 2002; Tessendorf et al. 2005; Wiens et al. 2005; Bruning et al. 2007; Deierling et al. 2008; Deierling and Petersen 2008; Lund et al. 2009; Schultz et al. 2009; Gatlin and Goodman 2010; Schultz et al. 2011, 2015). Recent key findings related to the lightning jump include that not only do graupel mass and  $10 \text{ ms}^{-1}$  updraft volume correspond well with flash rates, but that increases in these properties are markedly greater in flash rate increases that lead to lightning jumps versus non-jump increases (Schultz et al. 2015, 2016). Further definition of this relationship as it pertains to specific severe weather processes, particularly those enhanced by more complex downdraft interactions, requires a deeper understanding of thunderstorm microphysics and kinematics on finer spatial and temporal scales.

A thunderstorm's microphysics and kinematics fundamentally control its electrification and continued lightning production. The non-inductive charging mechanism, also referred to as the ice-graupel charging mechanism, is generally accepted as the dominant mode of thunderstorm electrification (Takahashi 1978, Stolzenburg et al. 1998). By this mechanism, charge is transferred between colliding ice and graupel particles in the presence of supercooled water. These charged particles then become separated by differences in fall speed combined with the influence of the updraft to establish primary charge regions. Related to thunderstorm microphysics, the polarity and magnitude of particle charging during collision are dictated by particle sizes, their relative

velocities, the temperature regions of the thunderstorm, and the effective liquid water content (Saunders et al. 1991, Saunders 1994, Saunders and Peck 1998). The tripole structure consisting of a main negative charge region surrounded by upper and lower positive charge regions is the most basic model of thunderstorm charge structure resulting from these processes, though more complex models relative to storm dynamics have been observed and described (e.g., Stolzenburg et al. 1998; Wiens et al. 2005; Tessendorf et al. 2007; Bruning et al. 2010; Calhoun et al. 2013). Lightning follows the establishment of charge regions as a result of the breakdown of increasing electric potential difference between them. Maintenance of these charge regions is thought to be aided by the updraft's contribution of mixed-phase precipitation mass and liquid water content that promote continued collisional charging (Carey and Rutledge 2000).

It is expected that the microphysical processes that contribute to lightning production also partially influence downdraft production and enhancement. Downdrafts are regions of negatively-buoyant air generated and driven in part by precipitation loading within the parent storm, evaporative cooling by entrainment of dry environmental air, cooling from melting of ice hydrometeors, and dynamical forcing (Hookings 1965; Srivastava et al. 1985, 1987; Rasmussen and Heymsfield 1987a,b; Knupp 1987, 1988; Vonnegut 1996; Tong et al. 1998; Naylor et al. 2012). The strength of the downdraft is dependent upon the combination of the strength of the updraft and its ability to provide and support precipitation mass included in the downdraft, ice and liquid microphysics within the storm, and the near-storm environment. Additionally, characteristics such as the location of downdrafts within storm structure are thought to be non-trivial. Specifically, the downdraft's composition and intensity can be influenced by the location and spatial distribution of hydrometeors within the storm. For instance, supercell thunderstorms are specifically characterized by two distinct downdraft regions; the rear flank downdraft (RFD) that originates from mean storm flow and pressure perturbations and is later influenced by precipitation, and the forward flank downdraft (FFD) that is driven more by

---

\*Corresponding author address: Sarah M. Stough, Univ. of Alabama in Huntsville, Dept. of Atmospheric Science, Huntsville, Alabama 35805-1912; email: sarah.stough@nsstc.uah.edu

precipitation loading (Lemon et al. 1979; Bluestein 1993; Markowski 2002; Markowski and Richardson 2010; Davies-Jones 2015).

Analysis of the hydrometeor fields in lightning flash initiation regions near the time of lightning jumps and their subsequent evolution may assist in characterizing the relationship between lightning and downdraft-related severe weather processes. The work presented here considers the three-dimensional spatial distribution and temporal evolution of hydrometeor fields related to lightning flash initiation locations near the time of lightning jumps. The microphysical characterization of specific lightning regions provides an additional perspective to the traditional storm-scale metrics of considering lightning flash rate evolution with respect to the microphysics of updraft processes.

## 2. DATA AND METHODS

This analysis considers three lightning jump periods from two supercell thunderstorms that occurred on different days. Polarimetric Doppler radar and three-dimensional total lightning mapping array (LMA) data constitute the primary data utilized in this study.

### 2.1 Radar data

The Advanced Radar for Meteorological and Operational Research (ARMOR, Schultz et al. 2012; Knupp et al. 2014) is a polarimetric C-band radar located at the Huntsville International Airport in Huntsville, AL. Reflectivity ( $Z_H$ ), differential reflectivity ( $Z_{DR}$ ), differential phase ( $\phi_{DP}$ ), and correlation coefficient ( $\rho_{HV}$ ) were the primary variables utilized. Data were processed following the Bringi et al. (2001) method for attenuation correction, differential attenuation correction, and calculation of specific differential phase ( $K_{DP}$ ). While polarimetric data from the S-band KHTX Weather Surveillance Radar-1988 Doppler (WSR-88D) were available for both cases, they were not analyzed in this study. Further work will employ data from both radars.

ARMOR data were utilized for the purpose of subjectively associating lightning flashes to individual storms, qualitative case assessment, and for hydrometeor identification (HID). ARMOR data were gridded using 0.5 km horizontal and vertical spacing with the Py-ART software (Helmus et al. 2016). HID was subsequently implemented according to the Dolan et al. (2009, 2013) algorithm, available as part of the CSU Radar Tools Python package (Dolan et al. 2002). Within the algorithm, the following weights were assigned to polarimetric variables and temperature data:  $Z_H=1.5$ ,  $Z_{DR}=1.2$ ,  $K_{DP}=1.0$ ,  $\rho_{HV}=0.4$ , and

temperature=0.4. These weights were modified from the default values based on sensitivity testing with ARMOR data. Temperature data for this use of the HID algorithm were obtained from a sounding launched from the National Weather Service (NWS) Warning and Forecast Office (WFO) in Nashville, Tennessee on 2 March 2012 at 1200 UTC and from a sounding launched from the University of Alabama in Huntsville on 31 March 2016 at 2300 UTC, applied to the 1 April 2016 analysis. HID data were used to compute graupel volumes as well as to characterize the regions in which lightning initiated. Graupel volume was obtained using the number of radar grid spaces identified by an HID graupel category, relating to the spatial volume containing graupel.

### 2.2 LMA data

Three-dimensional flash data were reconstructed from VHF sources obtained from the North Alabama Lightning Mapping Array (NALMA, Koshak et al. 2004; Goodman et al. 2005). The NALMA is a network of sensors that detect VHF sources emitted during lightning flashes.

Source data from the NALMA were grouped into flashes using spatial and temporal criteria according to the McCaul et al. (2009) flash-clustering algorithm. Lightning jumps were then computed from flash data using the Schultz et al. (2011) two-sigma lightning jump algorithm (LJA). Schultz et al. (2016) further describe the mathematical implementation of the algorithm, though briefly, a jump is considered to have occurred when the change in flash rate with time (DFRDT) at a specific two-minute time step of flash rate data is at least two times the standard deviation of the previous five DFRDT values. The value of each DFRDT relative to the standard deviation of the recent data is referred to as the sigma level. A lightning jump corresponds to a value of DFRDT with a sigma level  $\geq 2.0$ . However, when multiple rapid increases in flash rate with sigma levels  $\geq 2.0$  occur within a six-minute period, only the first is marked as a lightning jump.

In addition to the use of flash rate data, locations of flash initiation points were analyzed in space and time. Time-height cross-sections (THCSs) of flash initiations were analyzed in which flash initiation data were binned into 2-minute intervals and 0.5 km vertical spacing.

## 3. RESULTS

Three lightning jumps were analyzed from two separate supercell events in North Alabama that occurred on the morning of 2 March 2012 and

during the evening of 31 March 2016 (after 0000 UTC on 1 April 2016). Radar-based analyses corresponding to these lightning jumps began at three volume scans prior to the volume scan nearest the time of the jump and extended to the three following volume scans. ARMOR volume scans occurred in approximate four- to five-minute intervals for these cases. This segmentation of radar data allowed for analysis of microphysical evolution during the same approximate period over which flash data was considered when a jump was determined, matched by a similar period of observation of evolution following each jump.

### 3.1 2 March 2012

Three lightning jumps occurred during the total analysis period of the 2 March 2012 supercell, though only two were observed during the time that the storm was within 100 km of the center of the NALMA. Outside of 100 km, it is known that source location accuracy diminishes, with horizontal and vertical errors exceeding 500 m and 1000 m, respectively (Koshak et al. 2004). Source detection efficiency also suffers with range from the LMA center and flash detection efficiency begins to decrease below 96% outside of 100 km (Boccippio et al. 2001; Thomas et al. 2004; Carey et al. 2005; Chmielewski et al. 2016). The lightning flash rate and lightning jump data from the total storm analysis period are shown in Fig. 1.

### 3.1a 2 March 2012 – Jump 1

The first lightning jump occurred during the development of the supercell at 1446 UTC with a sigma level of 2.8. In this case, it is worth mentioning that although only one lightning jump was noted at 1446 UTC, a subsequent rapid increase in flash rate with a sigma level of 3.9 occurred at 1448 UTC as well. This period in the storm is characterized by intensification of the supercell, during which time the mesocyclone developed. Radar and HID analyses for this lightning jump occurred over the period from 1429 UTC to 1500 UTC.

A THCS of lightning initiation altitude during the analysis period is provided in Fig. 2. Prior to the time of the lightning jump, Figs. 1 and 2 illustrate that flash rates were low, at and below 10.0 flashes per minute (fpm). Most of the early flash initiation locations were near the height of  $-40^{\circ}\text{C}$ , as interpreted from the 12Z upper-air sounding launched from Nashville, TN. However, beginning approximately 10 minutes prior to the lightning jump, an increase in flash initiation locations near 3.5 km to 4.0 km was observed. At the time of the jump, the concentration of flashes initiating in this location greatly increased with maximum of 5.0 flash initiations observed near the height of  $-10^{\circ}\text{C}$ , corresponding to 4.7 km. Two primary regions of flash initiations persisted near 5.0 km and 8.5 km, corresponding roughly to the

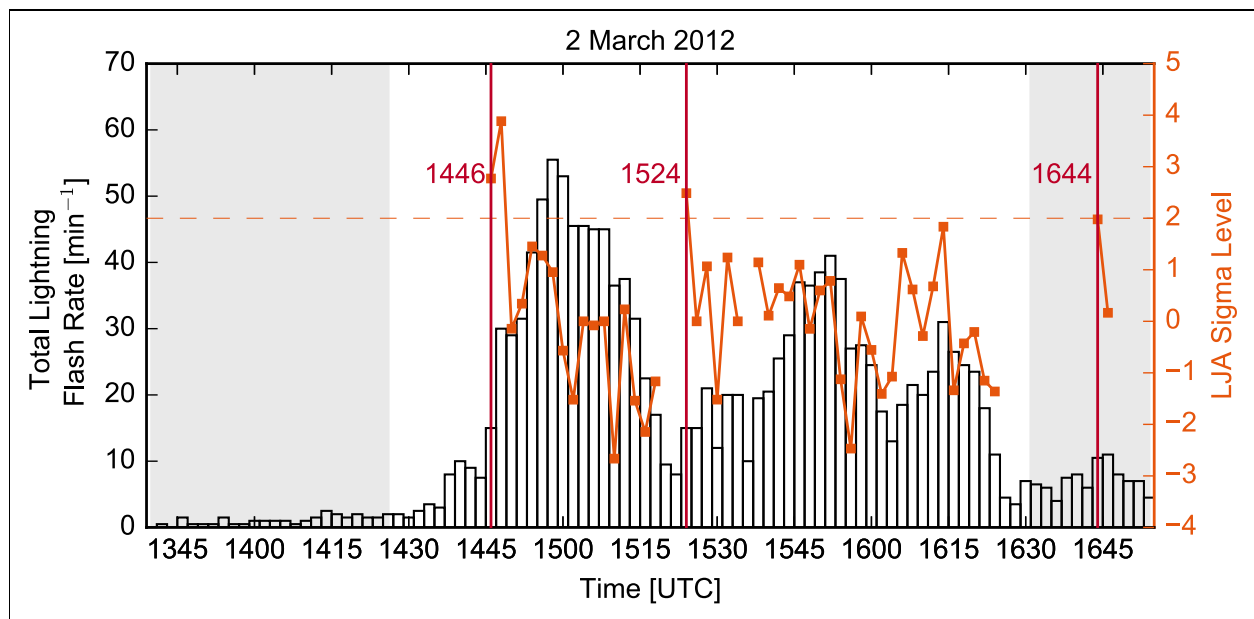


FIG. 1. NALMA total lightning flash rate and LJA information are provided for 2 March 2012. Two-minute binned flash rate is plotted in black, where grayed plot sections denote that the storm was between 100 km and 150 km from the NALMA center. Lightning jumps are marked as vertical red lines along with a time annotation. Sigma level is plotted as an orange line.

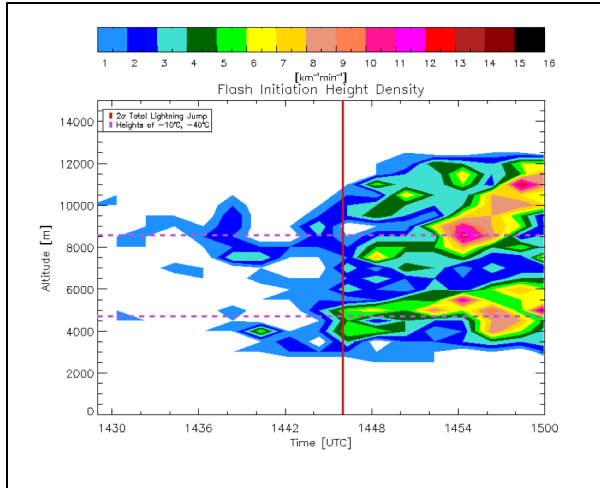


FIG. 2. THCS of lightning initiation altitude during the first lightning jump analysis period on 2 March 2012 is given as a density plot of lightning flash initiation locations. Image is color-filled according to the color bar at the top of the figure. The time of the lightning jump is plotted as a vertical red line. Heights of  $-10^{\circ}\text{C}$  and  $-40^{\circ}\text{C}$  are plotted as horizontal dashed purple lines.

heights of  $-10^{\circ}\text{C}$  and  $-40^{\circ}\text{C}$ , following the time of the jump.

THCSs of low-density (LD) and high-density (HD) graupel volume were also analyzed during the period, shown in Fig. 3. Leading up to the time of the lightning jump, the greatest volumes of HD graupel diminished. However, the greatest LD graupel volumes that were concentrated near 4.0 km increased in volume and expanded in altitude up to 6.0 km beginning 8 minutes prior to the lightning jump. Within 4 minutes following the lightning jump, the concentration of greatest LD graupel volume decreased in altitude and maximum LD graupel volume decreased. However, areas of moderate graupel volume  $40\text{ km}^3$  and greater expanded upward to 8.0 km. Simultaneously, the greatest concentrations of HD graupel volume diminished slightly and decreased in altitude by 1.0 km.

Examining the spatial context of the trends, Fig. 4 documents the horizontal distribution of lightning flash initiation locations through time in the 5.0 km and 8.0 km layers where most initiations were observed. In the period from 1429 UTC through 1434 UTC, prior to the time of the lightning jump, lightning initiations in the primary active layers occurred mostly at the

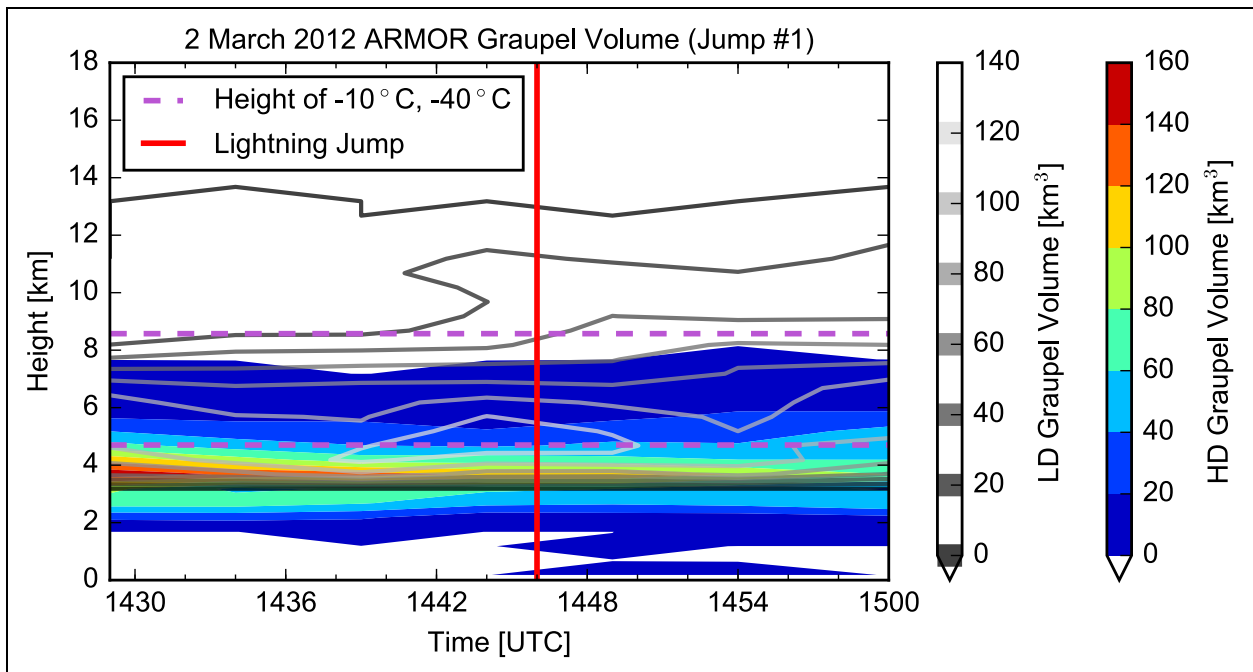


FIG. 3. THCS of LD and HD graupel volume during the first lightning jump analysis period of the 2 March 2012 event. HD graupel volume is contoured and color-filled according to the color bar on the right, while LD graupel volume is contoured in grayscale according to the color bar on the left. The time of the lightning jump is plotted as a vertical red line at 1446 UTC. Heights of  $-10^{\circ}\text{C}$  and  $-40^{\circ}\text{C}$  are plotted as dashed purple, horizontal lines.

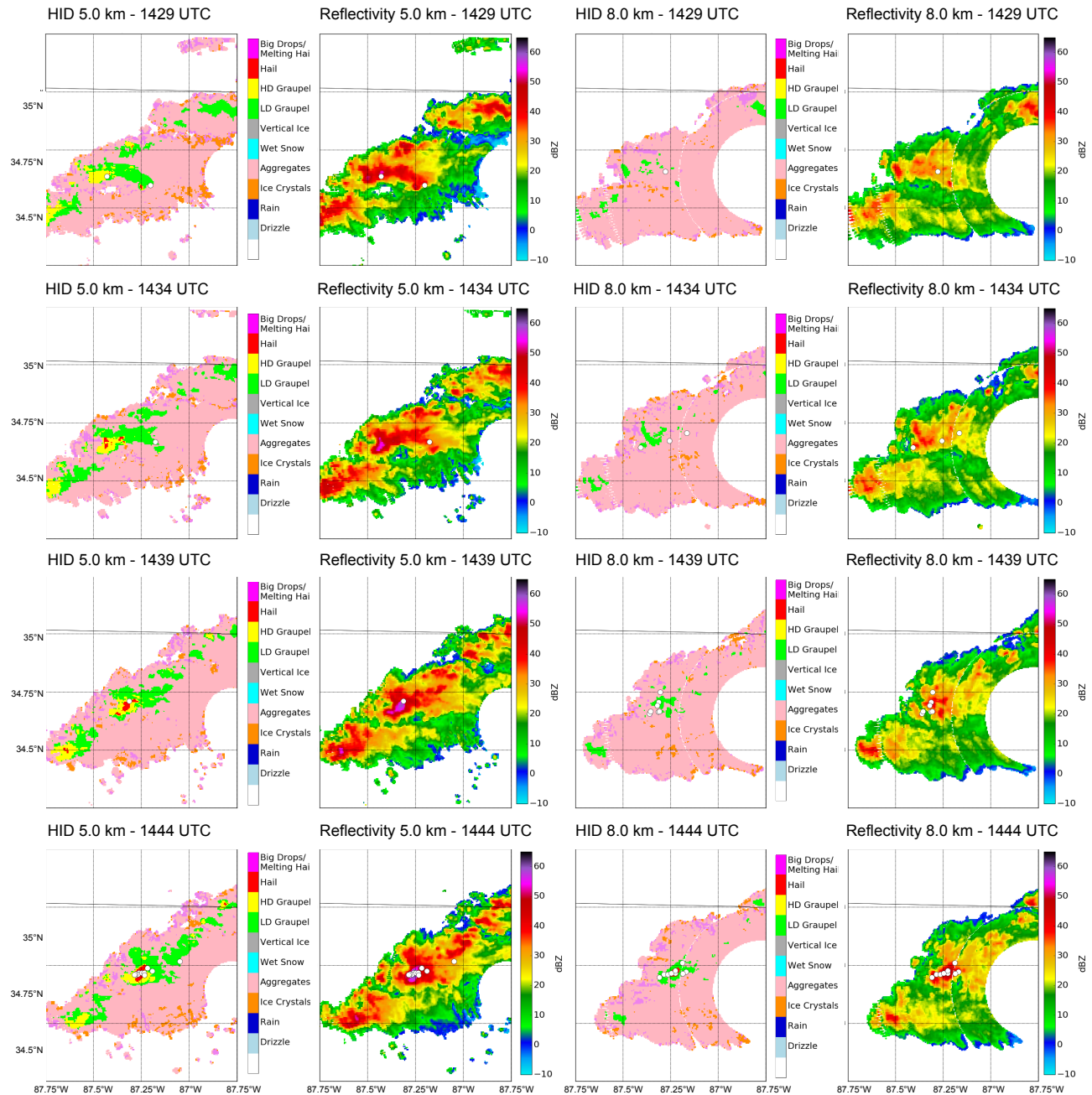


FIG. 4. Image depicts temporal evolution of HID in the 5.0 km layer in the left-most column, reflectivity in the 5.0 km layer in the left-center column, HID in the 8.0 km layer in the right-center column, and reflectivity in the 8.0 km layer in the right-most column. Rows depict the times from 1429 UTC through 1444 UTC, representative of the first half of the analysis period of the first lightning jump during the 2 March 2012 event. Lightning initiation points that occurred within 0.25 km of the level in the vertical are over-plotted as white circles. HID panels illustrated by HID score and reflectivity in dBZ are color-filled according to the provided color bars.

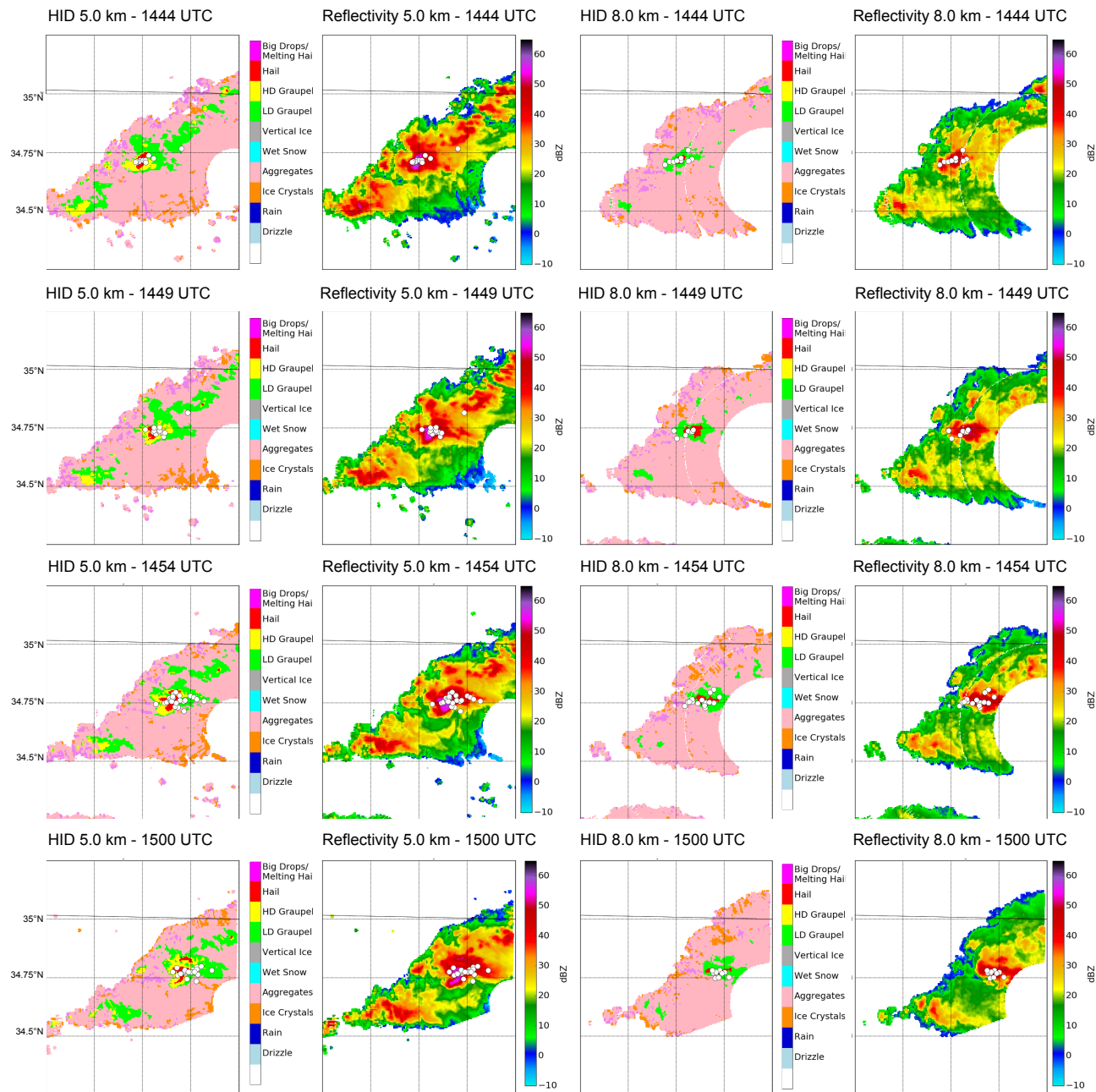


FIG. 4 (continued). Image depicts temporal evolution of HID in the 5.0 km layer in the left-most column, reflectivity in the 5.0 km layer in the left-center column, HID in the 8.0 km layer in the right-center column, and reflectivity in the 8.0 km layer in the right-most column. Rows depict the times from 1444 UTC through 1500 UTC, representative of the second half of the analysis period of the first lightning jump during the 2 March 2012 event. Note that the panels corresponding to 1444 UTC, closest to the time of the lightning jump, are repeated in this continuation for context. Lightning initiation points that occurred within 0.25 km of the level in the vertical are over-plotted as white circles. HID panels illustrated by HID score and reflectivity in dBZ are color-filled according to the provided color bars.

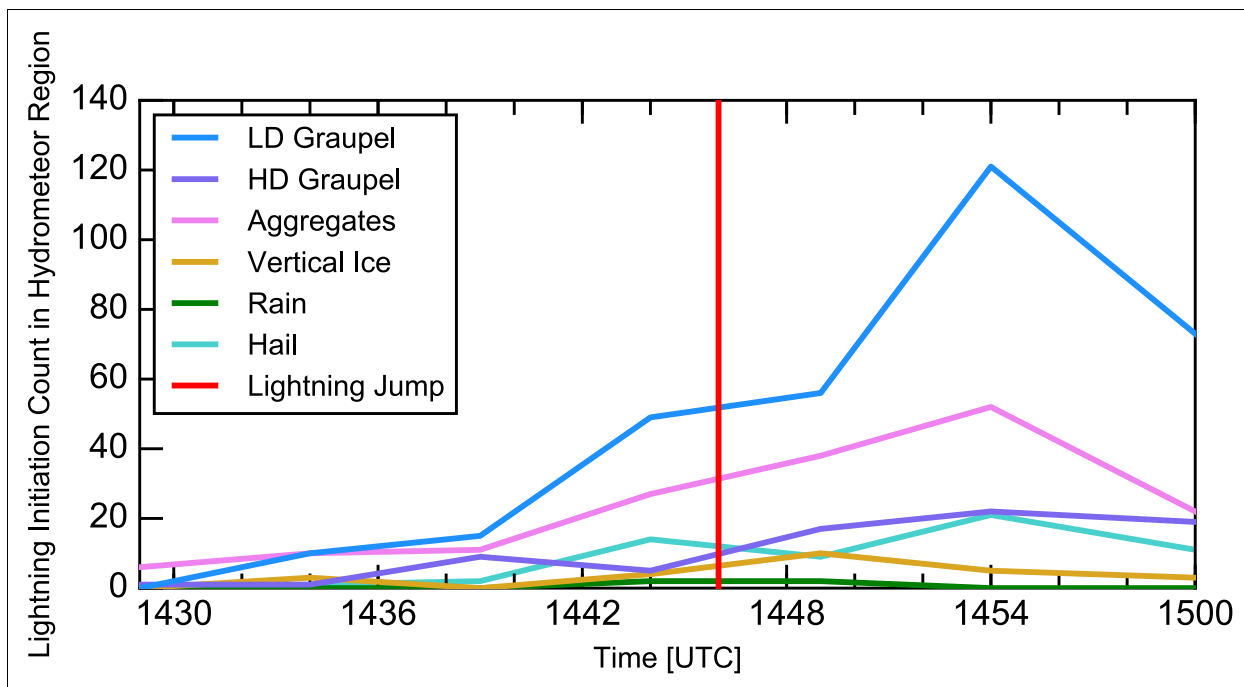


FIG. 5. Time series of the number of flash initiations observed in LD graupel, HD graupel, aggregate, vertical ice, hail, and rain regions of the 2 March 2012 supercell during the analysis period of the first lightning jump. The time of the lightning jump is marked by the vertical red line at 1446 UTC.

interface of the graupel and aggregate regions. From 1439 UTC, leading up to the jump and through the period following the jump at 1454 UTC, not only were more lightning initiations observed but most of the initiations were concentrated in the HD graupel and hail fields near the main updraft region of the storm. In the final two radar volumes of the lightning jump analysis period, lightning initiations began to disperse away from the main HD graupel and hail regions toward the LD graupel and aggregate fields.

Hydrometeor characterization of all lightning initiation points yielded that prior to the lightning jump, most flash initiations occurred in aggregate and LD graupel regions (Fig. 5). While there was some increase in the number of lightning initiations that occurred in the aggregate, hail, HD graupel, and vertical ice fields prior to the jump, the increase in the number of initiations in LD graupel regions was most substantial. Following the lightning jump, the number of flash initiations in LD graupel and aggregate regions continued to increase, and remained elevated until 1500 UTC at the end of the jump analysis period. Flash initiations in HD graupel and hail regions also continued to increase, though flash initiations in HD graupel regions did not decline near 1500 UTC

as the number of flash initiations in other hydrometeor fields did.

### 3.1b 2 March 2012 – Jump 2

The second lightning jump occurred at 1542 UTC with a sigma level of 2.5 following a decline and relative minimum in flash rate. The flash rate at the time of this lightning jump was similar to that of the first lightning jump at 15.0 fpm. Flash rate trends had recently been much higher at  $\geq 35.0$  fpm for a period of 20 minutes prior to this jump, during which the peak flash rate of 55.5 fpm occurred at 1458 UTC. Radar and HID analysis for this lightning jump correspond to the period from 1513 UTC to 1538 UTC.

Figure 6 depicts a THCS of flash initiation altitude corresponding to the second lightning jump analysis period. Relative to the first lightning jump analysis period, there are fewer flash initiations observed, though primary altitudes of initiation remain similar at approximately 4.5 km and 8.0 km. Unlike the first lightning jump period, most of the increase in initiation points occurred in the 8.0 km region near the height of  $-40^{\circ}\text{C}$  rather than near the height of  $-10^{\circ}\text{C}$ . Also unlike the first

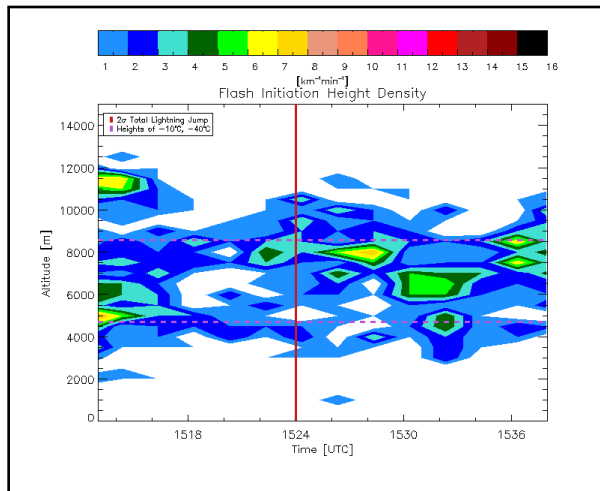


FIG. 6. THCS of lightning initiation altitude during the second lightning jump analysis period on 2 March 2012 is provided. Annotations are as described in Fig. 2 and the image is color-filled according to the key at the top of the figure. The lightning jump is plotted at the time of 1524 UTC.

lightning jump period, the strong bi-level characterization of flash initiations did not persist following the time of the lightning jump during the second period. A relative maximum in flash initiation altitude persisted near 8.0 km for approximately 6 minutes following the time of the

lightning jump, followed by a general decrease in all flash initiation altitudes and the development of a weaker relative maximum near 6.5 km.

HD and LD graupel volume during the analysis period of the second jump are shown in Fig. 7. Generally, graupel volumes were decreasing nearing the time of the second lightning jump. However, as with the first lightning jump, low to moderate LD graupel volumes of approximately 20 km<sup>3</sup> to 60 km<sup>3</sup> were expanding somewhat in height by 1.0 km to nearly 8.0 km and 10 km, respectively, leading up to the time of the lightning jump. Following the jump, narrow regions of the greatest LD and HD graupel volumes continued to diminish slightly, and heights of the greatest HD graupel volume also decreased in altitude by approximately 1.0 km, similar to what was observed following the first lightning jump.

Though most of the lightning initiations observed near the time of the second lightning jump took place near the 8.0 km region, the 5.0 km and 8.0 km layers are again shown in Fig. 8 from the second lightning jump period to allow for comparison between the two lightning jump periods. Prior to the second lightning jump, many of the flash initiations were again observed at the interface of the LD graupel and aggregate regions, particularly near the height of 8.0 km. Minutes before the lightning jump at 1524 UTC, radar and lightning imagery at 1520 UTC depict

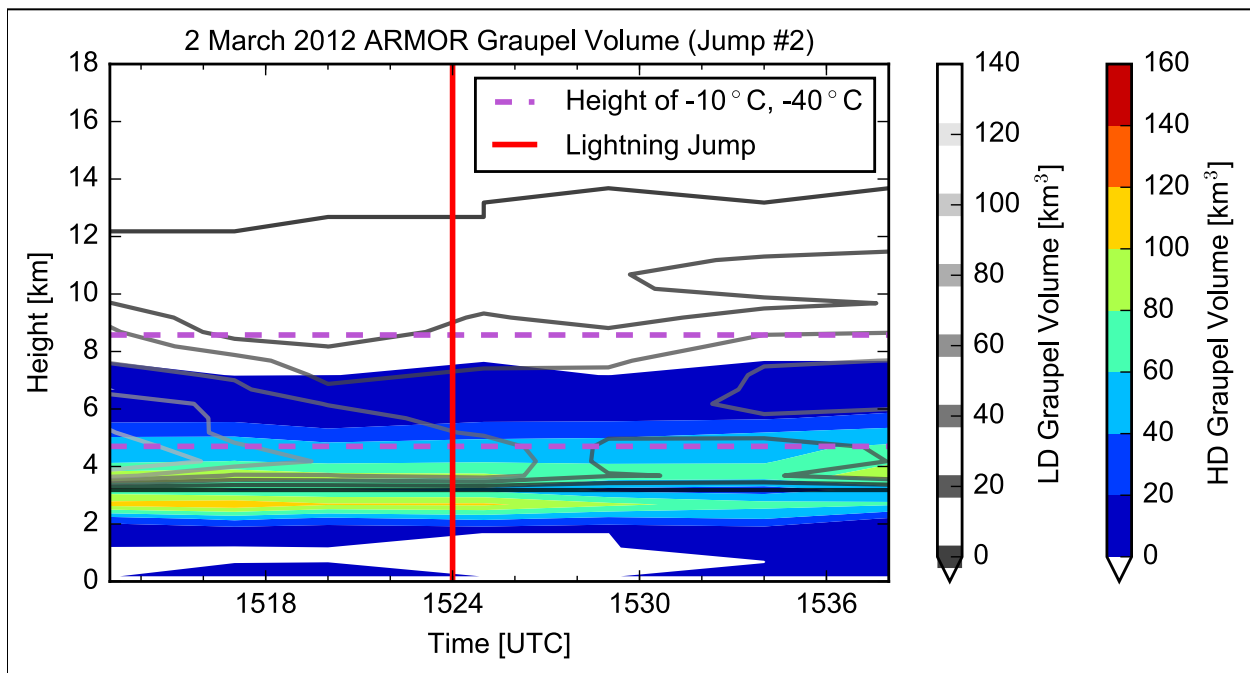


FIG. 7. THCS of LD and HD graupel volume during the second lightning jump analysis period of the 2 March 2012 event. Annotations, contours, and color fill are as described in Fig. 3. The time of the lightning jump is plotted as a vertical red line at 1524 UTC.

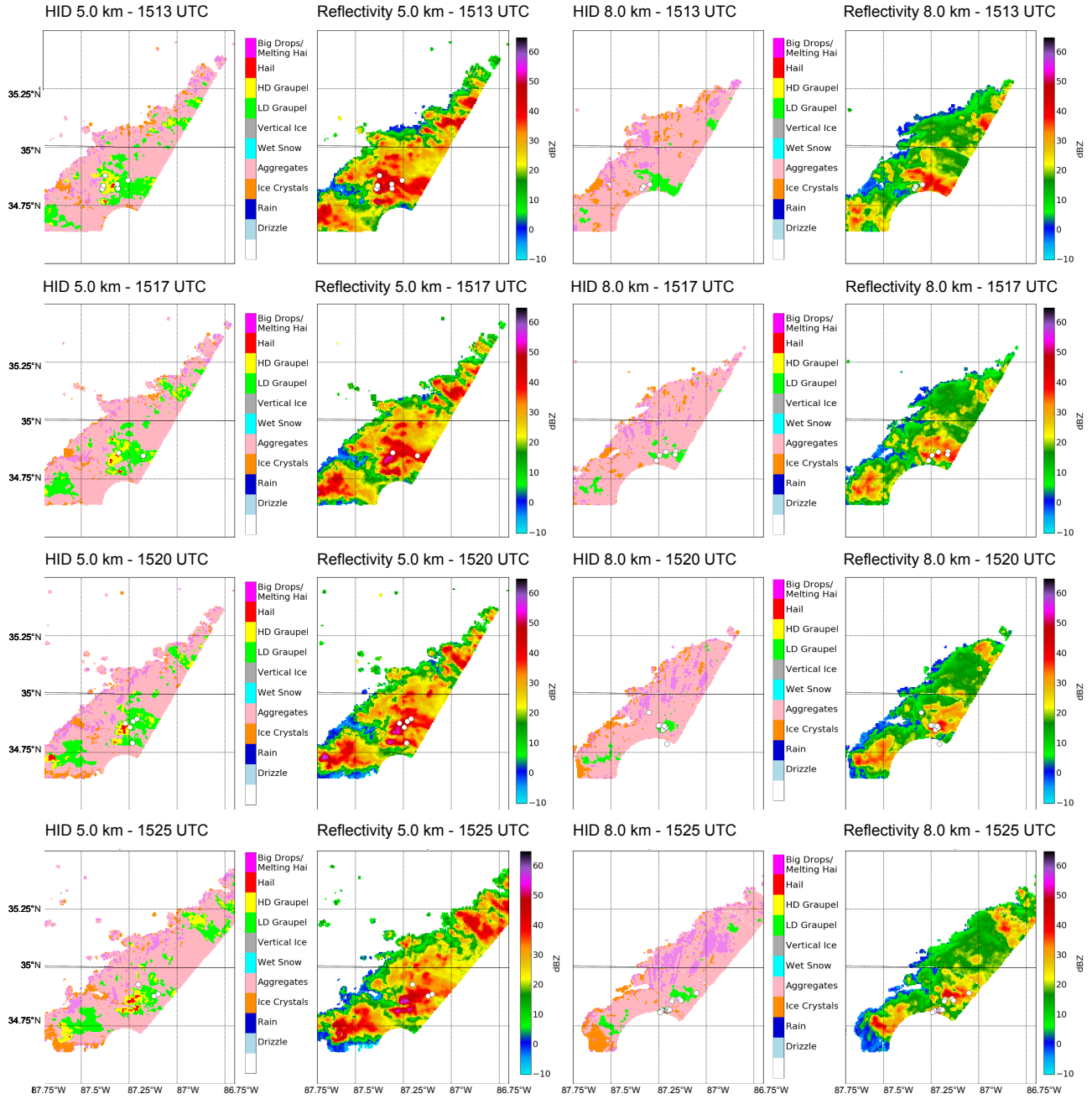


FIG. 8. Image depicts temporal evolution of HID and gridded reflectivity for the first half of the second lightning jump analysis period during the 2 March 2012 event from 1513 UTC through 1525 UTC. Layout, annotations, and shading are as described in Fig. 4.

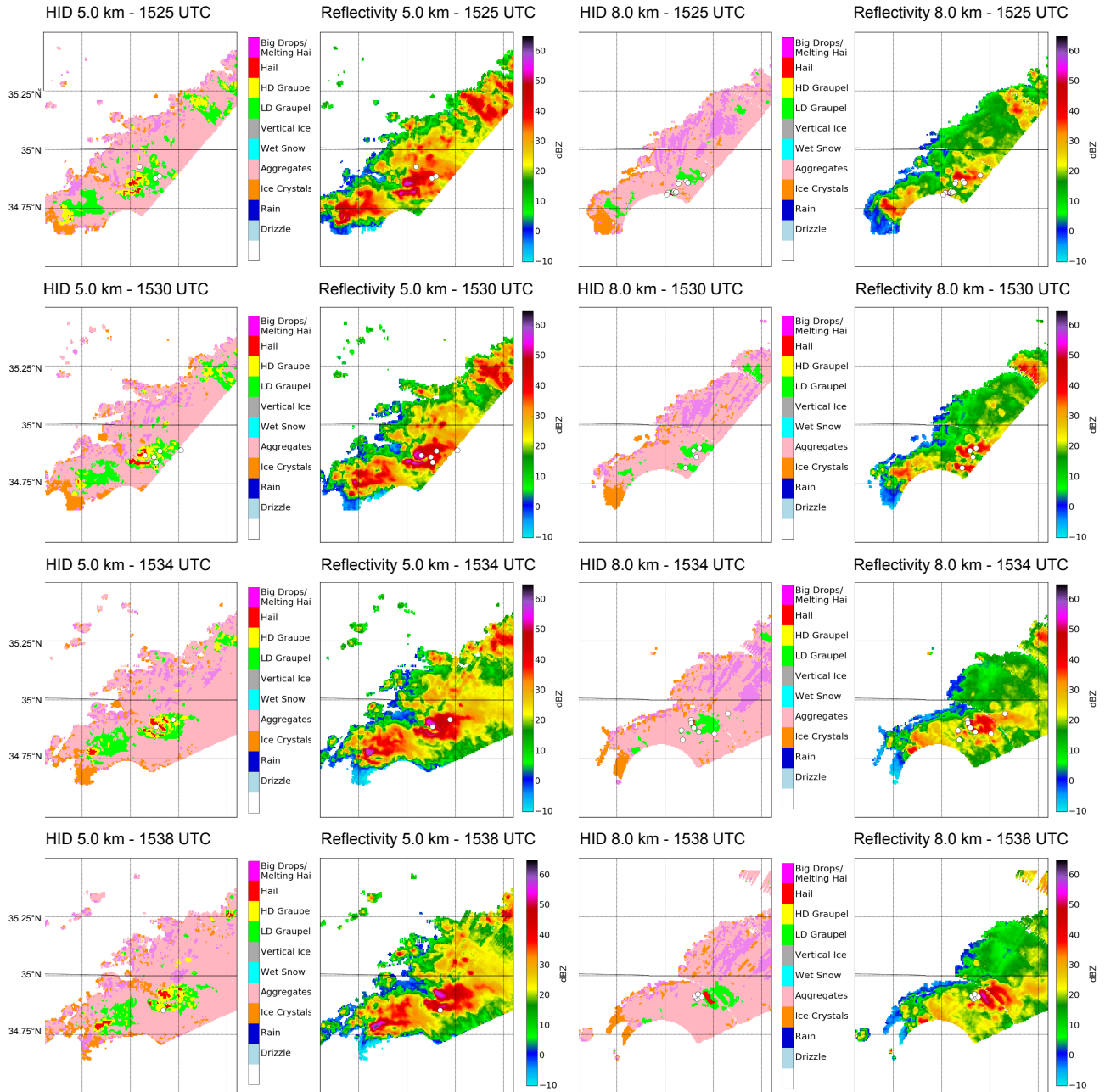


FIG. 8 (continued). Image depicts temporal evolution of HID and gridded reflectivity for the second half of the second lightning jump analysis period during the 2 March 2012 event from 1525 UTC through 1538 UTC. Note that the panels corresponding to 1525 UTC, closest to the time of the lightning jump, are repeated in this continuation for context. Layout, annotations, and shading are as described in Fig. 4.

more flash initiations in the LD graupel region near 5.0 km than observed prior to the first jump. Near the time of the second jump at 1525 UTC, there was a relative lack of initiation points near 5.0 km but many of the flash initiation points near 8.0 km were concentrated in and near LD graupel in pockets of higher reflectivity. This pattern continued from 10 minutes after the lightning jump at 1534 UTC to the end of the analysis period when initiations near the 8.0 km layer began to disperse toward aggregate regions once more. Relatively few lightning initiation points continued to be observed near 5.0 km.

Examining the time series of the hydrometeor characterization of lightning initiation locations in Fig. 9, it was apparent that flash initiations in aggregate regions were most prevalent during the analysis period, though the number of flash initiations associated with LD graupel showed the greatest increase prior to the lightning jump. The increase in LD graupel continued after the time of the lightning jump, its peak coincident with a low maximum in HD graupel volume at 1530 UTC. Contributions from other hydrometeor fields to lightning initiation counts were negligible.

### 3.2 1 April 2016

One lightning jump occurred during the storm analysis period of the 1 April 2016 supercell at 0140 UTC with a sigma level of 7.6. Radar and HID data were analyzed accordingly from 0126 UTC to 0156 UTC. A time series of the flash rate data from the period over which the entire supercell was analyzed is provided in Fig. 10. In contrast with the 2 March 2012 event, the maximum flash rate was relatively low at 27.0 fpm.

A THCS of flash initiations during the lightning jump analysis period (Fig. 11) depicts two primary levels of flash initiation near 8.0 km and 4.0 km. Unlike the 2 March 2012 event, these regions are not well-aligned with the heights of  $-40^{\circ}\text{C}$  or  $-10^{\circ}\text{C}$  at 9.9 km and 5.2 km. Prior to the time of the lightning jump, more lightning initiations generally occurred in the 8.0 km region. However, there was a moderate increase in flash initiations near 4.0 km beginning 6 minutes prior to the lightning jump and a more substantial increase in flash initiations between 6.5 km and 8.5 km within 4 minutes of the lightning jump. Following the lightning jump, the number of flash initiations in the 6.5 km to 8.5 km region increased and expanded

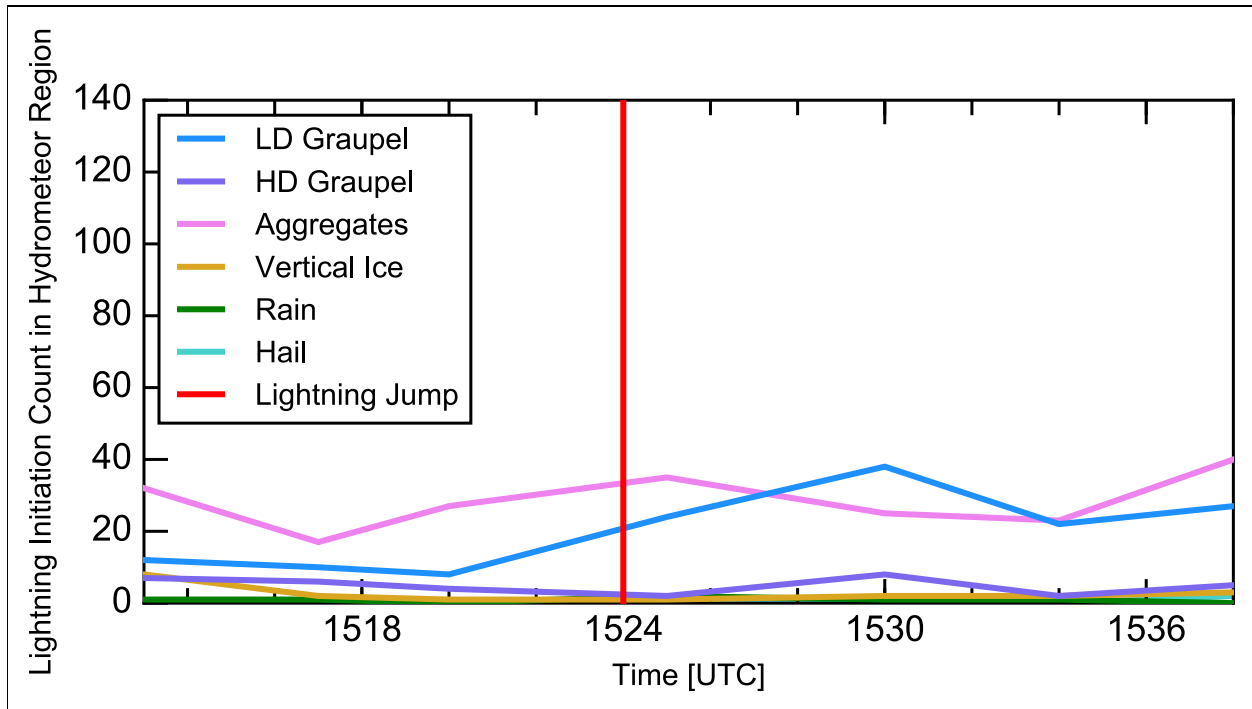


FIG. 9. Time series of the number of flash initiations observed in LD graupel, HD graupel, aggregate, vertical ice, hail, and rain regions of the 2 March 2012 supercell during the analysis period of the second lightning jump. The time of the lightning jump is marked by the vertical red line at 1446 UTC.

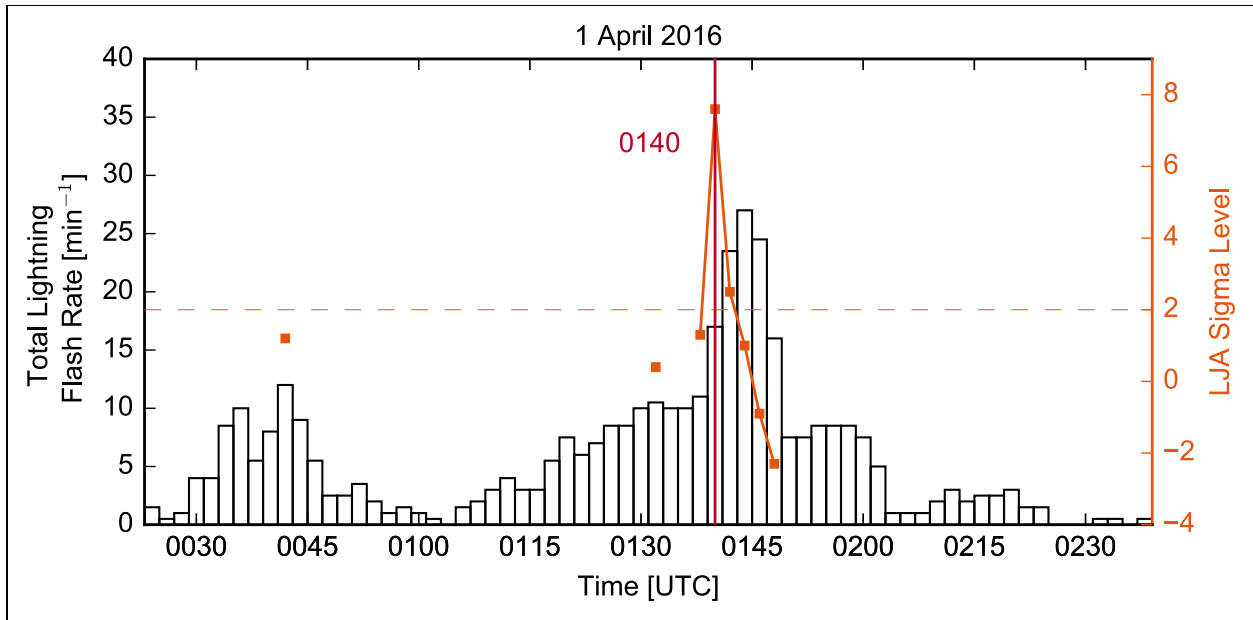


FIG. 10. As in Fig. 1 for the 1 April 2016 event.

to 6.0 km to 9.0 km. Flash initiations in the 4.0 km region experienced a brief reduction before increasing again at 0142 UTC.

HD and LD graupel THCSs for the 1 April 2016 lightning jump analysis period are provided in Fig. 12. The main concentrations of maximum LD and HD graupel volume were observed in close proximity near altitudes of 4.0 km to 5.0 km during the lightning jump analysis period. LD graupel volumes were relatively lower for this case, with maxima of less than  $60 \text{ km}^3$ . Unlike the 2 March 2012 lightning jump periods, the LD graupel volume was elevated prior to the jump and decreased during and following the jump. However, HD graupel volume was at a relative maximum 6 to 14 minutes prior to the jump, but reached a second relative maximum 2 minutes after the jump. HD graupel volume of greater than  $40 \text{ km}^3$  expanded in altitude within a minute of the lightning jump, but the region of greater volume ultimately decreased in altitude by 1.5 to 2.0 km following the lightning jump.

Horizontal cross-sections of the HID and reflectivity fields at 4.0 km and 8.0 km corresponding to the predominant flash initiation regions are provided in Fig. 13 for the lightning jump analysis period. Prior to the lightning jump, more flash initiations were observed near the 4.0 km layer than the 8.0 km layer. Of the flash initiations in the 8.0 km region, most were

associated with LD graupel and aggregate regions. Most flash initiations observed in the 4.0 km layer prior to the jump occurred either in LD graupel regions or at the interface of graupel and aggregate regions. Near the time of the lightning jump at 0141 UTC, more flash initiations in the 4.0 km layer occurred near HD graupel and hail regions of the FFD region of the supercell.

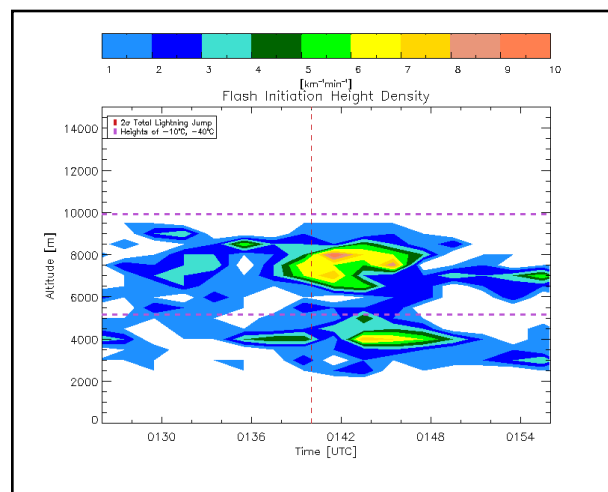


FIG. 11. THCS of lightning initiation altitude during the lightning jump analysis period on 1 April 2016 is provided. Annotations are as described in Fig. 2 and the image is color-filled according to the key at the top of the figure. The lightning jump is plotted at the time of 0140 UTC.

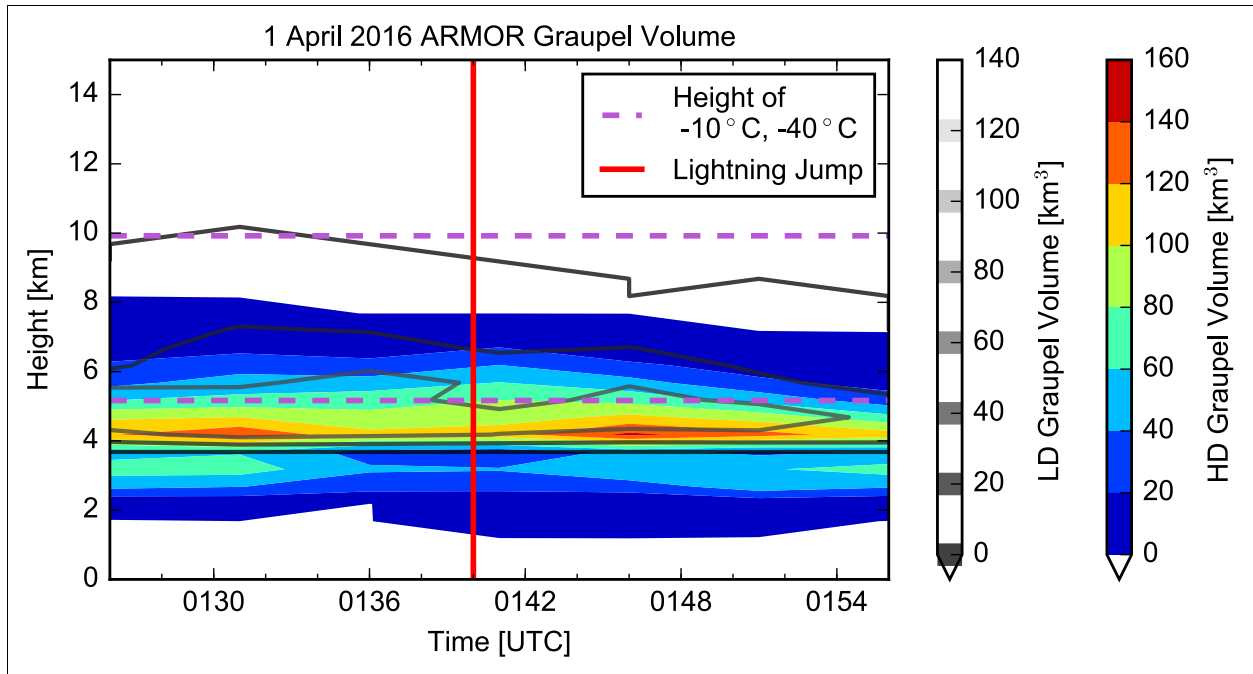


FIG. 12. THCS of LD and HD graupel volume during the lightning jump analysis period of the 1 April 2016 event. Annotations, contours, and color fill are as described in Fig. 3. The time of the lightning jump is plotted as a vertical red line at 0140 UTC.

Following the lightning jump, flash initiations in this layer dispersed throughout the HD graupel field and more of the FFD.

A time series of flash initiations associated with various HID fields during the lightning jump analysis period is shown in Fig. 14. Similar to the 2 March 2012 lightning jump analysis periods, aggregate and LD graupel characterizations dominated the flash initiation locations. However, flash initiations in HD graupel regions increased substantially along with flash initiations in LD graupel regions within 4 minutes of the lightning jump. Within the 6 minutes following the lightning jump, the number of flash initiations in LD graupel and aggregate regions decreased rapidly while the number of flash initiations in the HD graupel region decreased more gradually. There were a few more flash initiations in regions characterized by rain than observed during the 2 March 2012 lightning jump analysis periods. However, the temperature profile of the 1 April 2016 supercell was somewhat elevated in comparison with the 2 March 2012 supercell, suggesting a deeper warm layer where some flashes initiated. The 1 April 2016 supercell also displayed a substantial  $Z_{DR}$  column during this analysis period, indicative of the availability of

liquid hydrometeors above the melting level of 3.8 km (Vacek et al. 2016).

#### 4. DISCUSSION

For each of the three lightning jump analysis periods, lightning flash rates, spatial context of flash initiations, and evolution and spatial context of graupel volume within the storm were considered.

Comparing the two supercell storms, the 2 March 2012 supercell was demonstrably deeper with LD graupel volumes extending an additional 3.0 kilometers in altitude, indicative of a deeper mixed-phase region to promote increased electrification and charging. Flash rates between the two supercells were reflective of this with sustained maximum peak flash rates in excess of 40.0 fpm for over 20 minutes observed in the 2 March 2012 supercell compared with peak flash rates in excess of 15.0 fpm sustained for only 10 minutes in the 1 April 2016 case.

Because of the variation in thermodynamic profiles with respect to microphysical structure of the storms, their hydrometeor characterizations contrasted as defined by the concentration of greater graupel volume with altitude. Specifically,

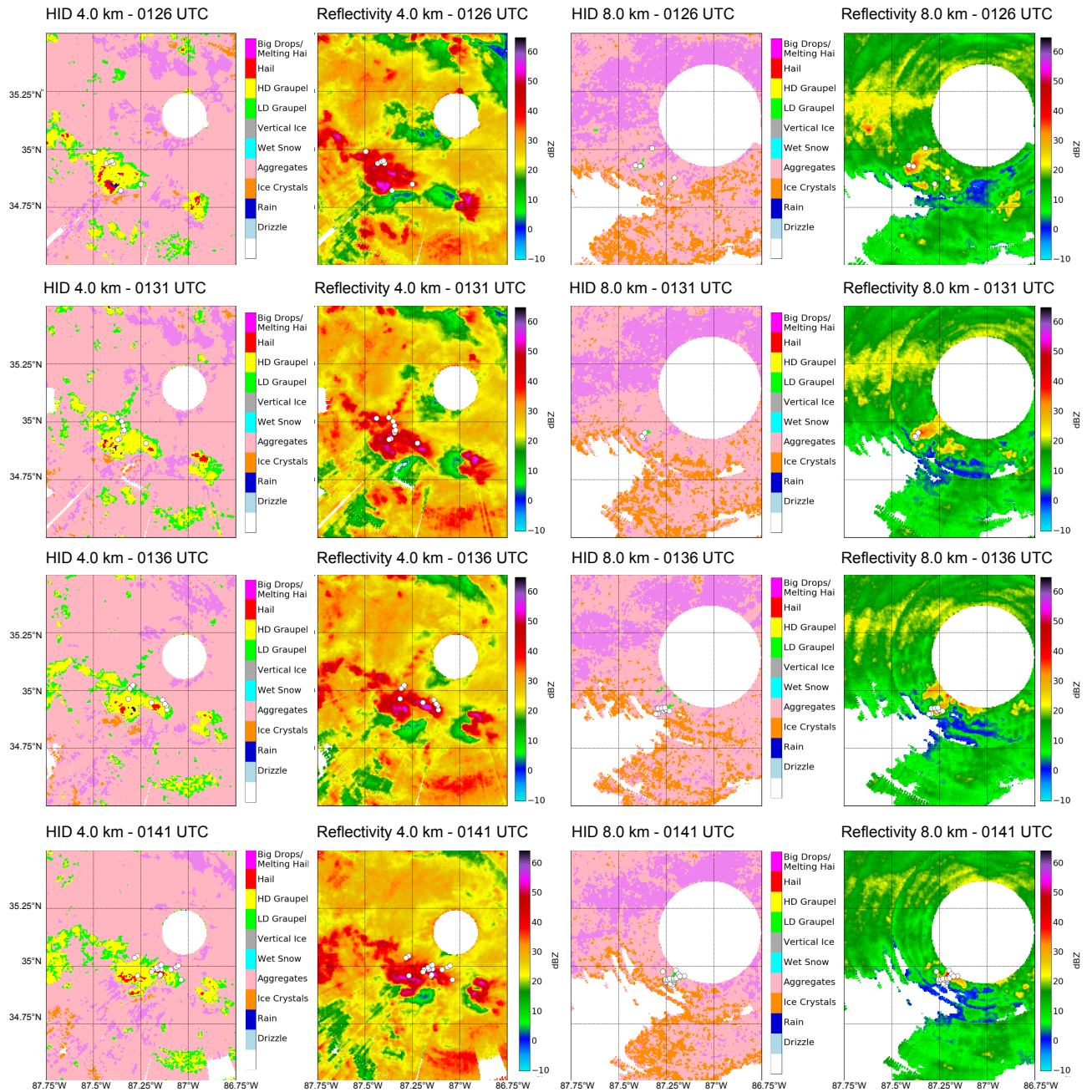


FIG. 13 Image depicts temporal evolution of HID in the 4.0 km layer in the left-most column, reflectivity in the 4.0 km layer in the left-center column, HID in the 8.0 km layer in the right-center column, and reflectivity in the 8.0 km layer in the right-most column. Rows depict the times from 0126 UTC through 0141 UTC, representative of the first half of the analysis period of the lightning jump during the 1 April 2016 event. Annotations and coloring are as described in Fig. 4.

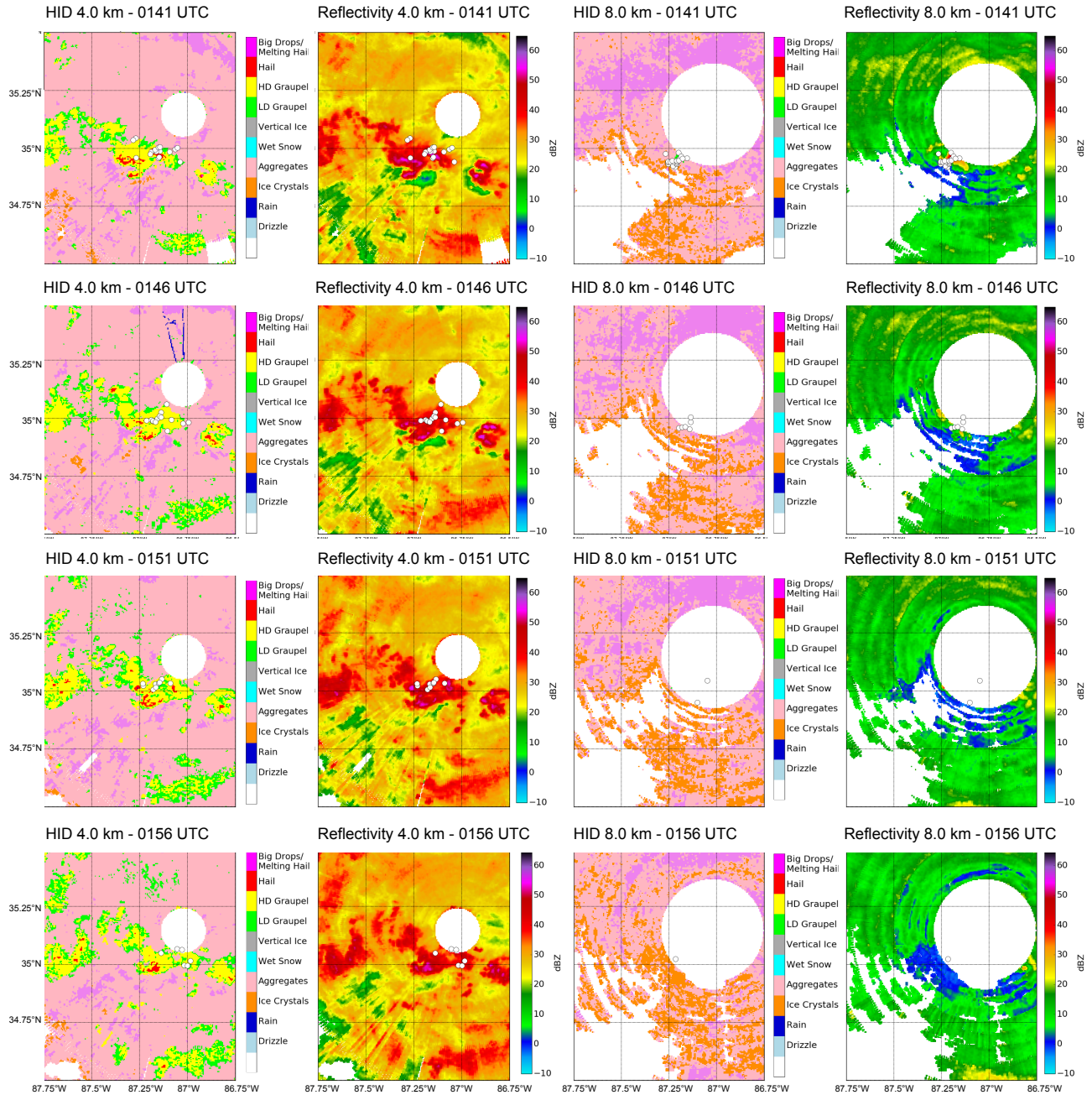


FIG. 13 (continued). Image depicts temporal evolution of HID in the 4.0 km layer in the left-most column, reflectivity in the 4.0 km layer in the left-center column, HID in the 8.0 km layer in the right-center column, and reflectivity in the 8.0 km layer in the right-most column. Rows depict the times from 0141 UTC through 0156 UTC, representative of the second half of the analysis period of the lightning jump during the 1 April 2016 event. Note that the panels corresponding to 0141 UTC, closest to the time of the lightning jump, are repeated in this continuation for context. Annotations and coloring are as described in Fig. 4.

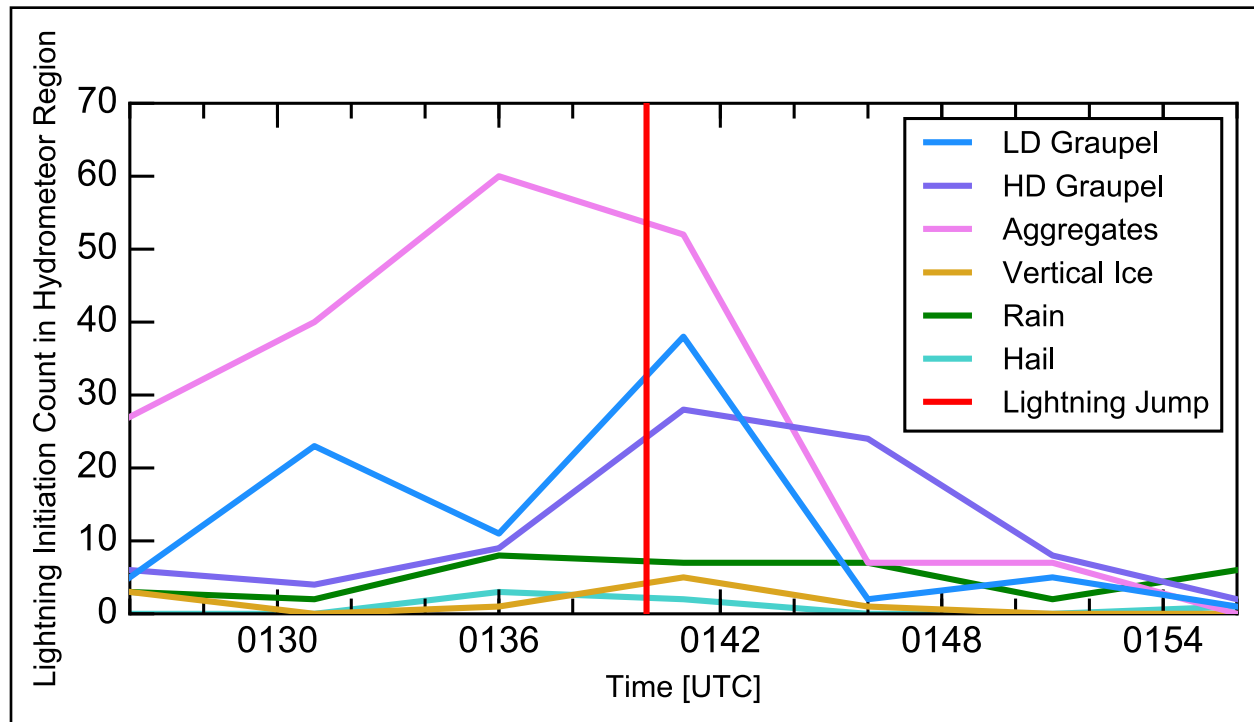


FIG. 14. Time series of the number of flash initiations observed in LD graupel, HD graupel, aggregate, vertical ice, hail, and rain regions of the 1 April 2016 supercell during the lightning jump analysis period. The time of the lightning jump is marked by the vertical red line at 0140 UTC.

whereas areas of greatest LD and HD graupel volumes were somewhat vertically separated in the 2 March 2012 case with maximum HD graupel extending from 1.0 km to 7.5 km and maximum LD graupel extending from 3.0 km to 13.0 km, maximum LD graupel volumes in the 1 April 2016 overlapped more in the vertical with HD graupel extending from 1.0 km to 8.0 km and LD graupel extending from 4.0 km to 10.0 km.

Though the vertical thermodynamic and microphysical structures of the supercells varied, both supercells demonstrated predominantly bi-level concentrations of flash initiations. This was particularly true of the first lightning jump analysis periods of each storm, whereas the second lightning jump analysis period of the 2 March 2012 storm was dominated by flash initiations in the upper level. The main regions of flash initiations in the 2 March 2012 supercell corresponded well with the  $-10^{\circ}\text{C}$  and  $-40^{\circ}\text{C}$  levels, presumably related to the interface of the lower positive and main negative charge regions and the main negative and upper positive charge regions, respectively, as represented in the traditional simplistic tripole charge structure of a thunderstorm. However, the main locations of

flash initiations within the 1 April 2016 supercell were more aligned with the  $0^{\circ}\text{C}$  to  $-2^{\circ}\text{C}$  region near 4.0 km and with the  $-25^{\circ}\text{C}$  region near 8.0 km. Further analysis of charge structure and flash polarity within this supercell as well as additional information from local soundings to verify the temperature profile are required prior to further interpretation.

When the hydrometeor types of flash initiation locations were identified during the jump analysis period, the characterization was analogous with findings from previous work in that most initiations occurred in graupel and aggregate regions. In all three lightning jump analysis periods, the number of initiations within graupel regions increased most substantially prior to the time of the lightning jump, as expected from the relationship between graupel mass increases and flash rate increases relative to the time of lightning jumps. In the 2 March 2012 lightning jumps, most of the graupel increase was categorized as LD, while flash initiations in HD graupel regions were almost as numerous as flash initiations in LD graupel regions leading to the jump in the 1 April 2016 case.

In each lightning jump analysis period, flash initiation location, HID, and reflectivity were

considered at the two primary levels of flash initiation over the duration of the period. In the lower levels during each lightning jump period, most initiations occurred at the periphery of graupel and aggregate regions leading up to the time of the jump. During each of the 2 March 2012 lightning jumps, in the radar volume during which the lightning jump took place and in subsequent volumes, more flash initiations occurred near the updraft region around graupel fields, and primarily HD graupel and hail regions when they were observed. In the 1 April 2016 lightning jump analysis period, the greatest concentration of flash initiations near 4.0 km was embedded within the FFD very near to a hail core to the northwest of the main updraft. After the time of the jump, flash initiations in all jump analysis periods typically dispersed throughout graupel regions within the FFD of the supercells. This was simultaneous with the minor descent of the main concentration of HD graupel within each storm following the lightning jump period. Considering upper primary level of flash initiations in each supercell at the time and shortly following each of the lightning jump, most flash initiations were concentrated near the updraft region of the storm and within the main associated LD graupel field. Whereas flash initiations in the lower primary levels of each lightning jump case tended to disperse throughout the FFD following the jump, flash initiations remained somewhat concentrated near the updraft post-jump, either within graupel regions or at the interface of the graupel and aggregate fields in the 2 March 2012 case. This behavior was coincident with the observed expansion of LD graupel volume with height in these two analysis periods. Conversely, flash initiations became more sparse in the upper layer within 6 minutes following the lightning jump and were less associated with LD graupel as LD graupel volumes also diminished in the same time period.

## 5. SUMMARY AND FUTURE WORK

In summary, three lightning jump periods within two supercell thunderstorms were analyzed with respect to the spatial distribution of flash initiation and hydrometeor characterization over a short period of time. It was generally observed that:

- Flash behavior was confined to two main levels during each lightning jump analysis period and that the spatial behavior of flash initiations with respect to

hydrometeor fields and supercell structure was similar between the two levels.

- In the lower of the two primary levels of flash initiations, initiations typically became more concentrated in the FFD near the updraft very near to the time of the lightning jump, associated primarily with HD graupel, LD graupel, and hail regions of the storms. Following the time of the jump, flashes in the lower levels dispersed throughout the graupel fields within the FFD.
- In the higher of the two primary levels of flash initiations, initiations tended to remain very near the updraft region, increasing in count near the time of the jump and remaining spatially associated with LD graupel and the interface between graupel and aggregate regions.
- Flash initiations associated with LD graupel in two lightning jumps and LD and HD graupel in one lightning jump increased in number most substantially leading up to the time of the jump compared with flash initiations in other hydrometeor regions.

This study presented a mostly qualitative assessment of the microphysical evolution of flash properties during the time of lightning jumps. While some inferences could be drawn related to kinematics, particle interactions, charging behavior based on the available observations, future work will particularly benefit from the addition of multi-Doppler analysis for the retrieval of three-dimensional winds, inclusion of S-band radar data for the benefit of hydrometeor characterization via another radar wavelength, as well as thunderstorm charge analysis. Flash extent information will also be considered in addition to flash initiation for a more in-depth characterization of the relationship between lightning and storm microphysical and kinematic structure.

Similar in-depth analysis of additional lightning jump periods will also be required to provide more data points relative to the general spatial and microphysical trends observed in these three lightning jump periods. When possible, radar measurements with finer temporal resolution would also assist in providing more detail relative to microphysical evolution.

## 6. ACKNOWLEDGMENTS

This work is supported by NASA A.25 Severe Storms Research (NNH14ZDA001N) and NASA MSFC Award NNM11AA01A.

## 7. REFERENCES

- Bluestein, H. B., 1993: Synoptic-Dynamic Meteorology in Midlatitudes Volume II: Observations and Theory of Weather Systems. Oxford University Press, Inc., 608 pp.
- Boccippio, D. J., S. Heckman, and S. J. Goodman, 2001: A diagnostic analysis of the Kennedy Space Center LDAR network, 1: Data characteristics. *J. Geophys. Res.*, **106**, 4769–4786, doi:10.1029/2000JD900687.
- Bringi, V. N., T. D. Keenan, V., Chandrasekar, 2001: Correcting C-Band radar reflectivity and differential reflectivity data for rain attenuation: A self-consistent method with constraints. *IEEE Trans. on Geo. and Rem. Sens.*, **39**, 1906-1915.
- Bruning, E. C., W. D. Rust, T. J. Schuur, D. R. MacGorman, P. R. Krehbiel, and W. Rison, 2007: Electrical and polarimetric radar observations of a multicell storm in TELEX. *Mon. Weather Rev.*, **135**, 2525–2544, doi: 10.1175/MWR3421.1.
- Bruning, E. C., W. D. Rust, D. R. MacGorman, M. I. Biggerstaff, and T. J. Schuur, 2010: Formation of charge structures in a supercell. *Mon. Weather Rev.*, **138**, 3740–3761, doi: 10.1175/2010MWR3160.1.
- Calhoun, K. M., D. R. MacGorman, C. L. Ziegler, and M. I. Biggerstaff, 2013: Evolution of lightning activity and storm charge relative to dual-Doppler analysis of a high-precipitation supercell storm. *Mon. Wea. Rev.*, **141** (7), 2199–2223, doi:10.1175/MWR-D-12-00258.1.
- Carey, L. D., M. J. Murphy, T. L. McCormick, and N. W. S. Demetriades, 2005: Lightning location relative to storm structure in a leading-line, trailing-stratiform mesoscale convective system. *J. Geophys. Res.*, **110** (3), 1–23, doi:10.1029/2003JD004371.
- Carey, L. D., and S. A. Rutledge, 1996: A multiparameter radar case study of the microphysical and kinematic evolution of a lightning producing storm. *Meteor. Atmos. Phys.*, **59**, 33–64, doi:10.1007/BF01032000.
- Carey, L. D., and S. A. Rutledge, 2000: The relationship between precipitation and lightning in tropical island convection: A C-band polarimetric radar study. *Mon. Wea. Rev.*, **128** (8), 2687–2710, doi: 10.1175/1520-0493(2000)128h2687:TRBPALi2.0.CO;2.
- Chmielewski, V. C., and E. C. Bruning, 2016: Lightning mapping array flash detection performance with variable receiver thresholds. *J. Geophys. Res.*, **121** (14), 8600–8614, doi: 10.1002/2016JD025159.
- Davies-Jones, R., 2015: A review of supercell and tornado dynamics. *Atmos. Res.*, **158-159**, 274–291, doi:10.1016/j.atmosres.2014.04.007.
- Deierling, W., and W. A. Petersen, 2008: Total lightning activity as an indicator of updraft characteristics. *J. Geophys. Res.*, **113**, D16210, doi:10.1029/2007JD009598.
- Deierling, W., W. A. Petersen, J. Latham, S. Ellis, and H. J. Christian, 2008: The relationship between lightning activity and ice fluxes in thunderstorms. *J. Geophys. Res.*, **113**, D15210, doi:10.1029/2007JD009700.
- Dolan, B., B. Fuchs, K. Wiens, R. Cifelli, L. Carey, T. Lang and Coauthors, 2002: CSU Radar Tools, accessed 2016. [Available online at [https://github.com/CSU-RadarMet/CSU\\_RadarTools](https://github.com/CSU-RadarMet/CSU_RadarTools).]
- Dolan, B., and S. A. Rutledge, 2009: A theory-based hydrometeor identification algorithm for X-band polarimetric radars. *J. Atmos. Ocean. Technol.*, **26**, 2071–2088, doi: 10.1175/2009JTECHA1208.1.
- Dolan, B., S. A. Rutledge, S. Lim, V. Chandrasekar, and M. Thurai, 2013: A robust C-band hydrometeor identification algorithm and application to a long-term polarimetric radar dataset. *J. Appl. Meteorol. Climatol.*, **52**, 2162–2186, doi:10.1175/JAMC-D-12-0275.1.

- Gatlin, P. N., and S. J. Goodman, 2010: A total lightning trending algorithm to identify severe thunderstorms. *J. Atmos. Ocean. Technol.*, **27** (1), 3–22, doi:10.1175/2009JTECHA1286.1.
- Goodman, S. J. and Coauthors, 2005: The North Alabama Lightning Mapping Array: Recent severe storm observations and future prospects. *Atmos. Res.*, **76**, 423–437.
- Helmus, J. J. & Collis, S. M., (2016). The Python ARM Radar Toolkit (Py-ART), a library for working with weather radar data in the Python programming language. *J. of Open Research Software*. **4** (1), p.e25. doi:http://doi.org/10.5334/jors.119.
- Hookings, G. A., 1965: Precipitation-maintained downdrafts. *J. Appl. Meteorol.*, **4**, 190–195.
- Knupp, K. R., and Coauthors, 2014: Meteorological Overview of the Devastating 27 April 2011 Tornado Outbreak. *Bull. Amer. Meteor. Soc.*, **95**, 1041–1062, doi: 10.1175/BAMS-D-11-00229.1.
- Koshak, W. J., and Coauthors, 2004: North Alabama Lightning Mapping Array (LMA): VHF source retrieval algorithm and error analyses. *J. Atmos. Ocean. Technol.*, **21** (4), 543–558, doi: 10.1175/1520-0426(2004)021<0543:NALMAL>2.0.CO;2.
- Lang, T. J., and S. A. Rutledge, 2002: Relationships between convective storm kinematics, precipitation, and lightning. *Mon. Wea. Rev.*, **130** (10), 2492–2506, doi: 10.1175/1520-0493(2002)130<2492:RBCSKP>2.0.CO;2.
- Lemon, L. R., and C. A. Doswell, 1979: Severe Thunderstorm Evolution and Mesocyclone Structure as Related to Tornadogenesis. *Mon. Wea. Rev.*, **107** (9), 1184–1197, doi: 10.1175/1520-0493(1979)107<1184:STEAMS>2.0.CO;2.
- Lund, N., D. MacGorman, T. Schuur, M. Biggerstaff, and D. Rust, 2009: Relationships between lightning location and polarimetric radar signatures in a small mesoscale convective system. *Mon. Wea. Rev.*, **137**, 4151–4170.
- MacGorman, D. R., D. W. Burgess, V. Mazur, W. D. Rust, W. L. Taylor, and B. C. Johnson, 1989: Lightning rates relative to tornadic storm evolution on 22 May 1981. *J. Atmos. Sci.*, **46** (2), 221–250, doi: 10.1175/1520-0469(1989)046<0221:LRRTTS>2.0.CO;2.
- Markowski, P. M., 2002: Hook echoes and rear-flank downdrafts: A review. *Mon. Wea. Rev.*, **130**, 852–876, doi: 10.1175/1520-0493(2002)130<0852:HEARFD>2.0.CO;2.
- Markowski, P., and Y. Richardson, 2010: Mesoscale Meteorology in Midlatitudes. John Wiley & Sons, Ltd, 407 pp.
- McCaul, E. W., S. J. Goodman, K. M. LaCasse, and D. J. Cecil, 2009: Forecasting lightning threat using cloud-resolving model simulations. *Weather Forecast.*, **24** (3), 709–729, doi:10.1175/2008WAF2222152.1.
- Naylor, J., M. A. Askelson, and M. S. Gilmore, 2012: Influence of low-level thermodynamic structure on the downdraft properties of simulated supercells. *Mon. Wea. Rev.*, **140**, 2575–2589, doi:10.1175/MWR-D-11-00200.1.
- Rasmussen, R. M., and A. J. Heymsfield, 1987a: Melting and shedding of graupel and hail. Part II: Sensitivity study. *J. Atmos. Sci.*, **44**, 2764–2782, doi: 10.1175/1520-0469(1987)044<2754:MASOGA>2.0.CO;2.
- Rasmussen, R. M., and A. J. Heymsfield, 1987b: Melting and shedding of graupel and hail. Part III: Investigation of the role of shed drops as hail embryos in the 1 August CCOPE severe storm. *J. Atmos. Sci.*, **44**, 2783–2803, doi: 10.1175/1520-0469(1987)044<2783:MASOGA>2.0.CO;2.
- Rison, W., R. J. Thomas, P. R. Krehbiel, T. Hamlin, and J. Harlin, 1999: A GPS-based three-dimensional lightning mapping system: Initial observations in Central New Mexico. *Geophys. Res. Lett.*, **26** (23), 3573–3576.
- Saunders, C. P. R., 1993: A review of thunderstorm electrification processes. *J. Appl. Meteor.*, **32**, 642–655.

- Saunders, C. P. R., 1994: Thunderstorm electrification laboratory experiments and charging mechanisms. *J. Geophys. Res.*, **99**, 10773–10779.
- Saunders, C. P. R., and S. L. Peck, 1998: Laboratory studies of the influence of the rime accretion rate on charge transfer during crystal/graupel collisions. *J. Geophys. Res.*, **103**, 13949, doi:10.1029/97JD02644.
- Saunders, C. P. R., W. D. Keith, and R. P. Mitzeva, 1991: The effect of liquid water on thunderstorm charging. *J. Geophys. Res.*, **96**, 7–11.
- Schultz, C. J., W. A. Petersen, and L. D. Carey, 2009: Preliminary development and evaluation of lightning jump algorithms for the real-time detection of severe weather. *J. Appl. Meteor. Climatol.*, **48** (12), 2543–2563, doi: 10.1175/2009JAMC2237.1.
- Schultz, C. J., W. A. Petersen, and L. D. Carey, 2011: Lightning and severe weather: A comparison between total and cloud-to-ground lightning trends. *Weather Forecast.*, **26** (5), 744–755, doi:10.1175/WAF-D-10-05026.1.
- Schultz, C. J. and Coauthors, 2012a: Dual-polarization tornadic debris signatures Part I: Examples and utility in an operational setting. *Electronic J. Operational Meteor.*, **13**, 120–137.
- Schultz, C. J., L. D. Carey, E. V. Schultz, and R. J. Blakeslee, 2015: Insight into the kinematic and microphysical processes that control lightning jumps. *Weather Forecast.*, **30**, doi: 10.1175/WAF-D-14-00147.1.
- Schultz, C. J., L. Carey, E. Schultz, and R. Blakeslee, 2016: Kinematic and microphysical significance of lightning jumps versus non-jump increases in total flash rate. *Weather Forecast.*, **32**, 275–288, doi: 10.1175/WAF-D-15-0175.1.
- Srivastava, R. C., 1987: A model of intense downdrafts driven by the melting and evaporation of precipitation. *J. Atmos. Sci.*, **44**, 1752–1774, doi: 10.1175/1520-0469(1987)044<1752:AMOIDD>2.0.CO;2.
- Stolzenburg, M., W. D. Rust, and T. C. Marshall, 1998: Electrical structure in thunderstorm convective regions: 3. Synthesis. *J. Geophys. Res.*, **103**, 14097–14108, doi: 10.1029/97JD03547.
- Takahashi, T., 1978: Riming electrification as a charge generation mechanism in thunderstorms. *J. Atmos. Sci.*, **35**, 1536–1548, doi:10.1175/1520-0469(1978)035<1536:REAA CG>2.0.CO;2.
- Tessendorf, S. A., L. J. Miller, K. C. Wiens, and S. A. Rutledge, 2005: The 29 June 2000 supercell observed during STEPS. Part I: Kinematics and microphysics. *J. Atmos. Sci.*, **62**, 4127–4150, doi:10.1175/JAS3585.1.
- Tessendorf, S. A., K. C. Wiens, and S. A. Rutledge, 2007: Radar and lightning observations of the 3 June 2000 electrically inverted storm from STEPS. *Mon. Wea. Rev.*, **135**, 3665–3681, doi: 10.1175/2006MWR1953.1.
- Thomas, R. J., P. R. Krehbiel, W. Rison, S. J. Hunyady, W. P. Winn, T. Hamlin, and J. Harlin, 2004: Accuracy of the lightning mapping array. *J. Geophys. Res.*, **109** (14), 1–34, doi: 10.1029/2004JD004549.
- Tong, H., V. Chandrasekar, K. R. Knupp, and J. Stalker, 1998: Multiparameter radar observations of time evolution of convective storms: Evaluation of water budgets and latent heating rates. *J. Atmos. Ocean. Technol.*, **15**, 1097–1109, doi: 10.1175/1520-0426(1998)015<1097:MROOTE>2.0.CO;2.
- Vacek, A. D., L. D. Carey and S. M. Stough, 2017: Kinematic, Microphysical and Lightning Properties of a Tornadic and Nontornadic Supercell during VORTEX-SE. Eighth Conf. on Meteorological Applications of Lightning Data, Seattle, WA. Amer. Met. Soc.
- Vonnegut, B., 1996: Importance of evaporative cooling in the formation of thundercloud downdrafts. *J. Appl. Meteorol.*, **35**, 1378.
- Wiens, K. C., S. A. Rutledge, and S. A. Tessendorf, 2005: The 29 June 2000 supercell observed during STEPS. Part II: Lightning and charge structure. *J. Atmos. Sci.*, **62**, 4151–4177, doi:10.1175/JAS3615.1.

Williams, E., and Coauthors, 1999: The behavior of total lightning activity in severe Florida thunderstorms. *Atmos. Res.*, **51** (3), 245–265, doi:10.1016/S0169-8095(99)00011-3.